Imaging biological structures with fluorescence photoactivation localization microscopy

Travis J Gould[1], Vladislav V Verkhusha[2] & Samuel T Hess[1]

[1]Department of Physics and Astronomy and Institute for Molecular Biophysics, University of Maine, Orono, Maine 04469, USA. [2]Department of Anatomy and Structural Biology and Gruss-Lipper Biophotonics Center, Albert Einstein College of Medicine, Bronx, New York 10461, USA. Correspondence should be addressed to S.T.H. (sam.hess@umit.maine.edu).

Published online 12 February 2009; doi:10.1038/nprot.2008.246

Fluorescence photoactivation localization microscopy (FPALM) images biological structures with subdiffraction-limited resolution. With repeated cycles of activation, readout and bleaching, large numbers of photoactivatable probes can be precisely localized to obtain a map (image) of labeled molecules with an effective resolution of tens of nanometers. FPALM has been applied to a variety of biological imaging applications, including membrane, cytoskeletal and cytosolic proteins in fixed and living cells. Molecular motions can be quantified. FPALM can also be applied to nonbiological samples, which can be labeled with photoactivatable probes. With emphasis on cellular imaging, we describe here the adaptation of a conventional widefield fluorescence microscope for FPALM and present step-by-step procedures to successfully obtain and analyze FPALM images. The fundamentals of this protocol may also be applicable to users of similar imaging techniques that apply localization of photoactivatable probes to achieve super-resolution. Once alignment of the setup has been completed, data acquisitions can be obtained in approximately 1–30 min and analyzed in approximately 0.5–4 h.

INTRODUCTION

With the resolution of light microscopy limited by the phenomenon of diffraction, fluorescence imaging of biological structures has been limited to length scales set by the Rayleigh criterion, $R_0=0.61\lambda/\mathrm{NA}$, where λ is the wavelength of detected light and NA is the numerical aperture[1]. Despite this limitation, fluorescence microscopy remains the most popular technique used in biological imaging applications[2]. The desire to observe biological structure and function at length scales smaller than R_0 has led to the development of imaging techniques that circumvent the diffraction barrier[2].

Recently, a revolution has begun in the field of far-field super-resolution imaging. The realization of stimulated emission depletion microscopy[3] first showed that resolution beyond the Rayleigh criterion could be attained in a light microscope. Stimulated emission depletion works by de-exciting molecules in the periphery of the focal volume before they emit fluorescence, resulting in a smaller effective observation volume. In contrast, a new class of microscopy techniques based on localization of single molecules uses optical control to activate a small subset of the molecules, find their positions and inactivate them in repeated cycles[4–6]. FPALM[4,7] and other localization-based methods circumvent the diffraction barrier by using repeated cycles of activation, localization and bleaching to localize (determine the position of) sets of single photoactivatable fluorescent tag molecules (**Fig. 1**). Once a sufficient number of these molecules have been imaged and localized, the measured molecular positions are plotted to generate an image. Essentially, FPALM exploits temporal multiplexing of molecular readout in addition to diffraction-limited spatial multiplexing. Rapid growth in this area has led to improvements in speed[8,9], extension to live cell imaging[7,10,11], multicolor imaging[12–14] and three-dimensional imaging[15–17] with effective lateral resolution better than 25 nm. Recently, the concept of FPALM has been extended to provide information about the orientation of single molecules[18].

As a further advantage, FPALM provides single-molecule information: brightness, number of photons emitted, intermittency, absolute numbers of molecules and molecular trajectories as a function of time[4–7,10]. In principle, it is also possible to determine emission spectra and fluorescence anisotropies of localized molecules. FPALM is suitable for imaging a wide variety of optically transparent samples with lateral resolution in the tens of nanometers. Samples can be living or fixed, biological or nonbiological, two-dimensional or three-dimensional. FPALM can image many samples that are amenable to widefield fluorescence, and can often improve the lateral resolution by tenfold or more.

Conceptually, FPALM, photoactivated localization microscopy (PALM)[5] and stochastic optical reconstruction microscopy (STORM)[6] are similar; PALM and STORM also use localization and reconstruction to generate super-resolution images. FPALM is typically implemented using a widefield fluorescence objective with high NA, which does not limit the focal plane to the proximity of the coverslip, although FPALM is compatible with total internal reflection fluorescence (TIRF) illumination[5]. PALM frequently (but not always) uses TIRF illumination of the sample. Using FPALM in the typical widefield geometry, three-dimensional samples can be imaged within a single focal plane of thickness approximately equal to the depth of field, achieving lateral resolution of tens of nanometers within that plane. Additionally, BP-FPALM[16] allows three-dimensional imaging of molecules in samples $\gg 1$ μm in thickness. In contrast, TIRF illumination limits the illuminated region of the sample to be within a few hundred nanometers of the coverslip surface, which reduces background fluorescence from out-of-focus molecules. STORM also uses a different type of probe to label the samples under reducing conditions (i.e., reduced levels of oxygen).

In FPALM and other localization-based methods, reliable localization of single fluorescent emitters requires that molecules be spatially separated well enough so that they can be distinguished from one another. Thus, for precise localization, no more than one molecule can be localized within each diffraction-limited area (A_{DL}, i.e., the area of the point-spread function) per frame, which

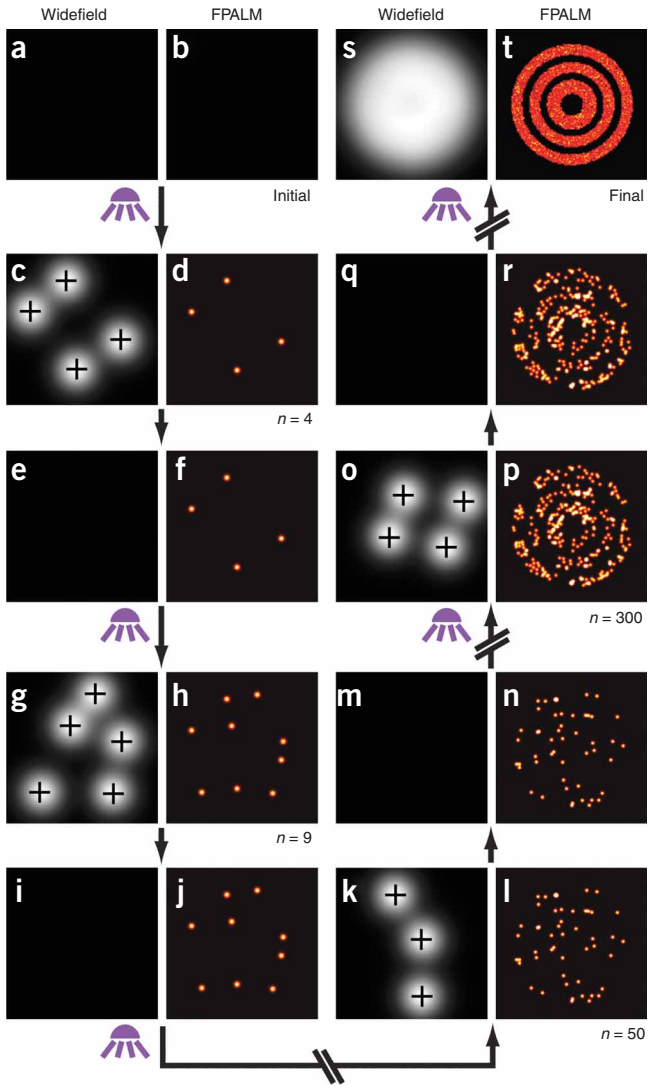

Figure 1 | Concept of FPALM. (**a**) Initially, photoactivatable probes are inactive and nonfluorescent under illumination by the readout laser (assumed to be continuous throughout) and (**b**) no molecules have been localized. After a pulse of illumination by the activation laser (purple light), (**c**) a sparse subset of molecules are activated and become fluorescent (bright spots) under the readout laser (on continuously). These active (fluorescent) molecules can be localized (black crosses) to start the buildup of the FPALM image, which is comprised of the plotted positions of all localized molecules (e.g., $n = 4$ in **d** and **f**). After the initial subset of (**e**) activated molecule bleaches, another subset of molecules is activated, (**g**) read out and (**i**) bleached to continue building the FPALM image ($n = 9$ in **h** and **j**). After many cycles of (**k**,**m**,**o**,**q**) activation, readout and bleaching, the FPALM image begins to show structures (**l**,**n**; $n = 50$) and shows the underlying configuration of molecules as the density of localized molecules increases (**p**,**r**; $n = 300$). After a large number of photoactivatable molecules ($n = 10{,}000$) have been activated, imaged and localized, (**t**) the FPALM image shows structures on subdiffraction length scales that are not resolvable in the (**s**) conventional widefield image. Images are simulated.

requires the acquisition of many images to obtain a high density of molecules in the final image. High density (such that the average nearest-neighbor distance is small) is necessary, as visualizing a structure contained within a certain area usually requires information from multiple molecules within that area. Both the precision with which the molecules can be localized and the nearest-neighbor distance between molecules determines the effective resolution of the image obtained[11]. If one molecule is localized per A_{DL} per frame, and A_{DL} is 250 nm × 250 nm in size, 100 optimized acquisition frames will yield at maximum 100 molecules within a box of area A_{DL}, resulting in an average nearest-neighbor distance of ~25 nm. In this case, where the localization precision is smaller than the nearest-neighbor distance (i.e., $\sigma \ll 25$ nm), the density of molecules limits the effective resolution, and ~25-nm effective resolution is possible at typical frame rates within times on the order of seconds, and potentially fractions of a second. The time resolution depends on the type of information and spatial resolution desired; individual molecular motions can be tracked if molecules are visible for more than one frame, with a time resolution equal to the time between frames, which is typically in the range of 3–100 ms. On the other hand, for a complete image of a region in the sample, at least n frames will be required to localize n molecules per A_{DL}. Clearly, for live-cell applications, the sample must not move significantly during the acquisition time. Also, the individual labeled molecules making up the structures of interest must not diffuse so much between frames that they cannot be localized due to significant blurring of the point spread function. Roughly, the mean squared displacement between frames should be less than or equal to A_{DL}.

Fluorescence photoactivation localization microscopy requires samples to be labeled with a specialized subset of fluorescent probes that are photoactivatable or photoswitchable, which include genetically encoded fluorescent proteins, caged or photoswitchable organic dyes and pairs of probes that act together as a molecular switch, such as those used in STORM[6,19]. Photoactivatable tags differ from conventional fluorescent tags in one crucial way: they are nonfluorescent (inactive) in the portion of the spectrum being imaged until they are photoactivated by a certain wavelength of light. Usually then, two excitation wavelengths are needed: one, called the activation wavelength, to photoactivate inactive molecules, and the second, called the readout wavelength, to image the active molecules. Ideally, inactive molecules are nonfluorescent even when illuminated by the readout laser. Thus, they are essentially invisible until activated, allowing the number of visible molecules to be tightly controlled such that the density of visible (fluorescent) molecules is low ('sparse') enough that individual molecules can be identified and localized. A variety of photoactivatable fluorescent tags are available. Most commonly, FPALM imaging has utilized either photoactivatable or photoswitchable fluorescent proteins as tags (collectively referred to here as PAFPs; see Experimental design), although caged organic dyes and photoswitchable pairs of organic dyes in close proximity are also usable as long as the conditions necessary for probe activation/inactivation are achieved.

Although a great variety of potential applications are accessible to FPALM imaging, certain ones may not be well suited. Submillisecond time resolution of molecular motions is limited by the excitation laser power, molecular emission rate and camera readout speed needed for submillisecond frame rates. For these reasons, acquisition of useful, complete FPALM data sets on time scales faster than ~0.1 s may be difficult to achieve. Also, imaging samples that emit significant autofluorescence in the same spectral region as the probe imposes limitations in localization precision,

TABLE 1 | Example calculations of two-dimensional localization precision in nanometers using equation 2 assuming 520-nm emission (e.g., PAGFP), 1.2 NA objective and 100-nm effective pixel size.

N (photons)	*b* (photons per pixel)			
	1	2	5	10
100	11.8	14.8	28.1	53.1
200	7.9	9.1	15.0	27.1
500	4.8	5.2	7.0	11.4
1,000	3.4	3.5	4.2	6.2
2,000	2.4	2.4	2.7	3.5

NA, numerical aperture; PAGFP, photoactivatable green fluorescent protein. Note that these calculations do not account for potential position errors arising from drift or nonuniform detection. These values also do not consider the efficiency of identification of molecules with a given total number of photons detected (*N*) and background noise per pixel (*b*).

which degrades rapidly with increasing background noise. In cases where background fluorescence is too large, the signal from a single fluorescent tag will not be distinguishable from the background.

Other situations reduce the suitability of FPALM for imaging and suggest using a different technique. Situations to avoid are as follows. (i) Using probes that do not emit many photons before photobleaching or have a slow rate of fluorescence emission (see **Table 1** for example calculations of localization precision using Eq. 2). Detecting <100 photons per molecule may also make it difficult to distinguish single molecules from the background. (ii) Imaging samples that require treatments incompatible with sensitive fluorescence detection. (iii) Imaging samples with so much scattering or absorption that widefield fluorescence imaging is not possible, or samples that cause optical phenomena that distort the detection point spread function.

Fluorescence photoactivation localization microscopy has potential for a great number of applications. Favorable situations and samples include the following (*Note*: this is not an exhaustive list): (i) optically transparent samples that can be labeled with photoactivatable probes, such as living or fixed cells, nanostructures or surfaces (samples do not need to be biological); (ii) intracellular or extracellular proteins tagged with PAFPs; (iii) biological membranes; (iv) cytoskeletal structures; (v) structures that can be labeled with (photoactivatable) fluorophore-tagged antibodies; (vi) cytoplasmic proteins; (vii) nuclear proteins; (viii) samples labeled with multiple (two or three) species with well-separated emission: combinations of one caged organic fluorophore with photoactivatable or photoswitchable fluorescent proteins[14].

Experimental design

Photoactivatable fluorescent proteins. Photoactivatable fluorescent proteins (PAFPs) are genetically encoded probes capable of substantial changes in their spectral properties in response to illumination with light of a specific wavelength, intensity or duration. As a result, some PAFPs convert from a dark (nonfluorescent) to a bright fluorescent form (called photoactivation), whereas others change their fluorescence emission wavelength (called photoswitching). These changes can be irreversible or reversible. PAFPs can be divided into three groups according to their photochemical properties[20]. **Table 2** compares some relevant properties of selected PAFPs.

The first group includes PAFPs capable of the irreversible photoconversion from the neutral (protonated) to anionic (deprotonated) form of the chromophore. Examples are PAGFP, which is the green fluorescent photoactivatable variant of *Aequoria victoria* GFP[21], photoswitchable cyan-to-green PSCFP and its enhanced PSCFP2 variant from *Aequorea coerulescens* jellyfish[22], as well as the photoactivatable red fluorescent proteins PAmRFP1[23] and PAmCherry[24], which are derived from the monomerized *Discosoma sp.* DsRed variants mRFP1 and mCherry, respectively. The proposed mechanism for photoconversion of this group of PAFPs is the decarboxylation of the Glu222 residue (amino-acid numbering is usually provided after alignment with GFP[20]) resulting in the reorganization of the hydrogen bond network inside the beta-barrel and eventual chromophore deprotonation[25]. Except for PAmRFP1, which has a tendency to dimerize, and tdEosFP, which is a single-chain dimer, all other PAFPs in this group are monomers. PAGFP was developed from GFP by introducing the single substitution of Thr203 to His, which produces the mostly neutral chromophore form[21,26]. In its inactive form, PAGFP has excitation/emission maxima at 400/515 nm, but the intensity of fluorescence is very low when inactive PAGFP is excited at wavelengths that correspond to the anionic chromophore form (e.g., 488 nm). However, intense violet-light irradiation (at or near 400 nm) leads to irreversible

TABLE 2 | Comparison of the properties of selected genetically encoded photoactivatable fluorescent proteins.

		Inactive form		Active form				
Protein	Activation light	Peak abs. (nm)	Peak em. (nm)	Peak abs. (nm)	Peak em. (nm)	Reversible	Oligomeric state	Reference
PAGFP	UV-violet	400	515	504	517	No	Monomer	21
Kaede	UV-violet	508	518	572	580	No	Tetramer	27
PSCFP2	UV-violet	400	470	490	511	No	Monomer	31
tdEosFP	UV-violet	506	516	569	581	No	Tandem dimer	28
Dendra2	UV-violet or blue	490	507	553	573	No	Monomer	31
Dronpa	UV-violet	390	n/a[a]	503	518	Yes	Monomer	33
PAmRFP1-1	UV-violet	385	n/a[b]	578	605	No	Monomer	23
KFP1	Green	450	n/a[b]	590	600	Yes or no	Tetramer	32
KikGR	UV-violet	507	517	583	593	No	Tetramer	29
PAmCherry	UV-violet	404	n/a[b]	564	595	No	Monomer	24

[a]Dronpa is inactivated (converted into a dim state) by strong excitation at 490 nm and regains fluorescence under ~400-nm illumination. [b]Weak or negligible emission of these probes is observed in the inactive form.

photoconversion of the PAGFP chromophore from the neutral to the anionic form, which is excited at 504 nm and emits at 517 nm. PAGFP photoconversion results in a 100-fold increase in the green fluorescence of the anionic form[21]. In contrast to PAGFP, the ground states of the PSCFP and PSCFP2 are characterized by a cyan fluorescence with excitation/emission peaks at 400/470 nm. Intense violet-light irradiation of PSCFP2 results in a 400-fold increase in green fluorescence, with excitation/emission maxima at 490/511 nm and a respective fivefold decrease in cyan (470 nm) emission. As compared with parental mRFP1 and mCherry, the main amino-acid substitutions resulting in PAmRFP1 and PAmCherry are at positions 148, 165 and 203. Several reported PAmRFP1 variants initially have a dim cyan fluorescence but after irreversible photoactivation exhibit up to 70-fold increase in red fluorescence *in vitro*, with excitation and emission peaks at 578/605 nm (see ref. 23). PAmCherry is nonfluorescent in the ground state, with its chromophore in a protonated state, but violet-light illumination converts it into an anionic bright red state. This photoconversion results in excitation/emission maxima at 564/595 nm and a photoactivation contrast (see below) of 4,000-fold.

The second group of PAFPs is capable of an irreversible photoconversion of the chromophore from a green to red fluorescent state due to a polypeptide backbone break next to the chromophore, which is followed by the formation of an additional chemical bond in the chromophore. This group consists of PAFPs from Anthozoan corals, such as tetrameric Kaede from *Trachyphyllia geoffroyi*[27], tetrameric EosFP (and its tandem dimeric tdEosFP and monomeric mEosFP variants) from *Lobophyllia hemprichii*[28], KikGR derived from green fluorescent protein KikG from *Favia favus*[29] and monomeric Dendra[30] and improved Dendra2[31] from *Dendronephthya sp.* dendGFP. The chromophores of these PAFPs are formed by the tripeptide His65-Tyr66-Gly67. The unique positioning of His at position 65 is responsible for the formation of the photoconvertable green chromophore. Intense UV-violet light irradiation induces a cleavage of the backbone between the amide nitrogen and the Cα of His65 and a double-bond formation between the Cα and Cβ of His65. The extension of a system of conjugated double bonds results in a red shift of the fluorescence emission.

The third group consists of PAFPs capable of either reversible or irreversible photoconversion from a dark state to the fluorescent state. The group includes a kindling red fluorescent protein KFP1 designed on the basis of asulCP chromoprotein from the *Anemonia sulcata*[32] and the dark-to-green Dronpa[33] family with its enhanced mutants, including rsFastLime[34], Dronpa-M159T (also named Dronpa-2) and Dronpa-3 from *Pectiniidae sp.* coral[35]. The proposed mechanism for the reversible photoconversion (kindling), which occurs at rather moderate intensities of photoactivating light, is a *trans*-to-*cis* chromophore isomerization followed by chromophore deprotonation. The fluorescent anionic chromophore of Dronpa emits photons in the green region with excitation/emission peaks at 503/518 nm. Irradiation with blue light (e.g., 488 nm) leads to protein quenching into a nonfluorescent protonated state with an absorption maximum at 388 nm. Dronpa can then be reversibly converted back to a fluorescent state by irradiation at 400 nm. The enhanced rsFastLime, Dronpa-M159T, and Dronpa-3 mutants are characterized by faster response to 488-nm light and by faster thermal relaxation from a dark state to the fluorescent state. The activation–quenching events can be repeated up to hundreds of times for KFP1 and the Dronpa variants. Intense violet-light irradiation results in an irreversible photoactivation of KFP1. KFP1 is an obligate tetramer, whereas Dronpa variants are generally monomers.

Selection of PAFPs for cell imaging by FPALM. For localization-based imaging methods, such as FPALM, both the biochemical and the photophysical characteristics of PAFPs should be considered carefully. The PAFP construct should also be codon-optimized for expression in the cell line or organism being used.

Although the desired photophysical properties for FPALM are specialized, the biochemical properties of PAFPs to consider are generally the same as those for ensemble imaging. These include PAFP oligomeric state, pH stability and efficiency and rate of chromophore formation. Monomeric and, sometimes, single-chain tandem dimeric PAFPs can be used for protein tagging, whereas organelles and cells can also be labeled with nonlinked dimeric and tetrameric PAFPs. However, PAFP dimerization and tetramerization may cause incorrect protein labeling patterns and can affect biological function in living cells. The best approach is to compare the labeling pattern with results from immunostaining using antibodies against the labeled protein. It is also possible to compare with the labeling pattern of the monomerized variant of EGFP[36], which contains the Ala126-to-Lys substitution. Data on the molecular weight of the purified PAFP as compared with monomeric EGFP, the dimeric version of DsRed or dTomato and the tetrameric DsRed standards in native polyacrylamide gel may also be helpful to check the oligomeric state. A high pH stability of PAFP fluorescence is important for reliable FPALM imaging in acidic organelles, such as late and recycling endosomes, lysosomes and the Golgi complex. For the highest PAFP brightness, generally pH > pKa. PAFPs that quickly form a functional chromophore capable of photoactivation (also known as chromophore maturation) will reduce delay between gene expression and imaging in live cells. Efficient chromophore maturation at 37 °C (or appropriate incubation temperature for the given biological system) is required to achieve an effective labeling of fusion proteins. If the efficiency of PAFP chromophore formation is low at this temperature, only a fraction of the proteins tagged with the PAFP will allow for photoconversion. For example, in the case of monomeric red PAFPs, mEosFP fails to efficiently form its chromophore at 37 °C (see ref. 28). On the other hand, Dendra2 and PAmCherry completely form the functional chromophore at this temperature.

The photophysical properties most desirable for FPALM include those affecting the spatial resolution and speed of image acquisition. The resolution of FPALM is a function of the localization precision achievable for any single fluorescent molecule imaged and the density of molecules localized within the structure of interest. As the localization precision improves with increased number of detected photons per molecule, PAFPs that emit as large a number of photons as possible before bleaching are desirable. The total number of photons detected (N) on average is proportional to such ensemble parameters of the PAFP as its extinction coefficient, quantum yield and photostability. However, not only a large N, but also a high rate of photon emission is important for fast FPALM imaging. Faster acquisition minimizes the impact of sample drift and is crucial for live-cell imaging. Saturation typically limits the maximum emission rate per molecule, and therefore selection of probes for FPALM should also consider maximum detected count

rate per molecule, when available. Higher PAFP photon emission rates allow for the detection of more photons in shorter acquisition times and hence better localization precision at high acquisition frame rates. Therefore, PAFPs with good photostability, efficient photoconversion, large N and high rate of photon emission per molecule should provide the best spatial resolution in fixed cells.

Another parameter that can greatly limit (or assist) FPALM imaging is the readout-induced activation yield (ϕ_{RA}), which is the probability per readout-laser photon absorbed that the molecule will become activated (in the absence of activation light). Readout-induced activation not only allows FPALM to be carried out using a single-laser wavelength[4,8,37], but also reduces control over the number of visible molecules within the region of interest (ROI). If $\phi_{RA} > 0$, molecules will activate in the readout laser beam, and if the distance between active molecules gets too small, localization of individual molecules is no longer possible, and the principle of FPALM breaks down. As a remedy, the user can bleach the sample until the density of molecules decreases (after significant depletion of the inactive pool of molecules), but then the number of molecules localized will be much less than the total number of photoactivatable probes, and the overall density of molecules in the final image will be suboptimal. Generally, it is advantageous to choose PAFPs with as small a ϕ_{RA} value as possible, whenever data are available.

The achievable localization precision will also be affected by photoactivation contrast, which reflects the relative change in PAFP molecular brightness upon photoactivation (i.e., the brightness ratio of inactive and active forms under the conditions used to detect the active form). In practice, the detected background signal increases if inactive molecules are even weakly fluorescent in the same detection range as the active molecules. Therefore, other parameters being the same, PAFPs with larger photoactivation contrast will provide higher localization precision.

For FPALM imaging in live cells, where the speed of image acquisition becomes critical to visualizing the dynamics of intracellular events, several additional PAFP parameters become important. Low PAFP saturation intensities and long-lived dark states can potentially slow the FPALM imaging cycles. Generally, as long as readout-induced activation does not cause significant numbers of visible molecules with overlapping images, higher readout intensity will lead to higher photobleaching rates, and higher emission rates below fluorescence saturation. The speed of FPALM acquisition can also be affected by the rate of PAFP photoactivation (sometimes referred to as 'PAFP softness'). Although this is not usually a limitation, the faster the PAFP can be activated, the faster the cycles of activation-readout-bleaching can be performed and images obtained. Various intermittent dark (nonfluorescent) states of activated PAFPs (e.g., blinking and flickering) due to chromophore photochromism, chromophore isomerization, protonation–deprotonation events[38–41] and triplet states can lead to reduced numbers of localized molecules, reduced apparent intensities of molecules and slower acquisition. Depending on the application, reappearance of the fluorescent PAFP from its dark state can also complicate data analysis. Overall, brighter PAFPs with faster photobleaching rates, faster photoactivation rates and minimal dark state interconversion should be considered.

Microscope objective lens. Use a high NA objective lens to improve collection efficiency and reduce R_0 (i.e., maximize conventional resolution; see INTRODUCTION). Although oil-immersion lenses (NA $\geq$ 1.4) provide higher NA than water-immersion lenses (NA $\sim$1.2), water-immersion objectives have the advantage of reducing spherical aberrations arising from index of refraction mismatch when imaging samples in water through a glass coverslip. Slightly lower-NA objectives also reduce localization errors due to probe polarization and orientation effects[42]. The magnification of the objective lens should be chosen such that the effective pixel size at the sample (the physical size of the camera pixels divided by the total magnification) is small enough so that the image of a single molecule is (roughly) at least two pixels wide, to minimize localization errors due to pixel size[43]. If necessary, an additional pair of lenses positioned as a telescope in the detection path in front of the camera can be used to provide additional magnification (see **Fig. 2**).

Camera calibration. Calculating the precision with which a molecule is localized requires the knowledge of the number of photons detected from the molecule. Pixel values in the offset-subtracted images obtained by the camera are proportional to the number of detected photons and can be used to estimate the number of fluorescence signal photons after background subtraction and camera calibration for the particular gain settings used during an acquisition. To calibrate the camera intensity scale at a given gain setting, obtain images of a temporally stable, incoherent

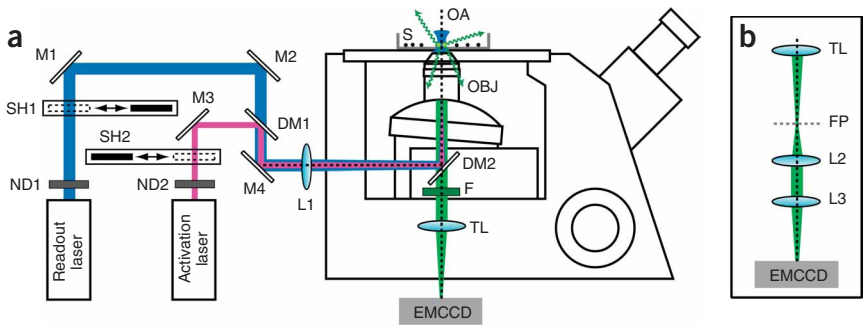

Figure 2 | FPALM experimental setup. (**a**) The readout laser is directed into the microscope stand using mirrors M1, M2 and M4, whereas mirror M3 and dichroic mirror DM1 provide freedom of adjustment to align the activation laser to be collinear with the readout laser along the optical axis (OA, dashed line). Both lasers are focused by lens L1 located near the back port of the microscope and directed to the objective lens (OBJ) by dichroic mirror DM2 to illuminate sample S labeled with photoactive probes. Fluorescence from the sample is collected by OBJ, separated from laser light by DM2, band-pass filtered (F) and focused by the tube lens (TL) to form an image on the EMCCD camera sensor. Laser intensities at the sample are controlled using neutral-density filters ND1 and ND2. Shutters SH1 and SH2 allow on/off control of the readout and activation lasers, respectively. (**b**) Additional lenses (L2 and L3 with focal lengths f_2 and f_3, respectively) arranged as a telescope in the detection path may be added to increase the total magnification. The original focal plane (FP) of TL is now imaged onto the EMCCD camera with a lateral magnification equal to the ratios of the focal lengths, f_3/f_2 times the original magnification.

light source transmitted through the field aperture under Koehler illumination at several different intensities, covering the dynamic (linear) range of the camera. Calculate the mean pixel value and variance of a region that is uniformly illuminated at each intensity. Plot variance as a function of mean pixel value and find the slope of the best-fit straight line. This slope is approximately the ratio of registered pixel value per detected photon[43]. The offset corresponding to zero light (i.e., the dark counts) of the camera can be measured by acquiring an image with the camera shutter closed (at a specific electron multiplying (EM) gain and exposure time).

Lasers and filter combinations. The choice of activation and readout lasers depends on the activation/excitation properties of the PAFP used, although near-UV activation is typical for most PAFPs (see above and **Table 2**). The readout laser should be chosen also to supply enough excitation intensity for single molecules to emit enough photons to be distinguishable from the background. (See sample calculation of number of expected detected photons per frame, **Box 1**.) Choose a dichroic mirror to combine the activation and readout beams onto a collinear path. When using near-UV activation, a Z405RDC dichroic mirror (Chroma) is usually adequate for readout lasers with wavelengths from 430 to 650 nm. Choose emission filter combinations (dichroic mirror + band-pass filter, mounted within the microscope filter turret) to maximize reflection (dichroic) and absorption (emission filter) of both lasers, while transmitting as much fluorescence from the sample as possible. For example, imaging Dendra2 is possible using 405-nm activation (BCL-405-15, Crystalaser) and 556-nm readout (LRS-556-NM-100-10, Laserglow.com) with probe emission separated from laser light using a T565LP dichroic mirror (Chroma) and ET605/70M band-pass filter (Chroma). Activation/excitation/emission properties of PAFPs can be obtained from their original references (see above) and in recent review articles[20,44]. In general, using readout wavelengths as close to the excitation maximum as possible will maximize the emission rate of molecules, given a certain intensity of excitation light. Excitation with a wavelength much shorter than the maximum can sometimes increase photobleaching, although this is not always the case. Depending on the particular cell type, the readout laser wavelength should be chosen to reduce excitation of background. Although there is no general rule for the best wavelength (this depends on the cell type and PAFP combination), autofluorescence in mammalian cell lines is sometimes lower when exciting and detecting at longer wavelengths.

BOX 1 | ESTIMATING THE FRAME RATE FOR A GIVEN NUMBER OF DETECTED PHOTONS

Note: these calculations will yield order-of-magnitude estimates, not precise values. They are intended for making a very rough estimate of the acquisition time per frame (frame rate) needed to detect a certain number of photons from a single species of fluorescent molecules. These calculations do not take into account saturation effects, which will become significant at high excitation rates.

The rate of photons detected from a single molecule (f_{det}) can be estimated by

$$f_{det} = k_x \phi_{fl} \phi_{det} \quad (B1)$$

where k_x is the excitation rate of that species, ϕ_{fl} is the fluorescence quantum yield and ϕ_{det} is the detection efficiency (typically 0.02–0.05, i.e., 2–5%). The excitation rate can be calculated using

$$k_x = \sigma I \quad (B2)$$

where σ is the excitation cross-section (units of cm^2) and I is the intensity (units of photons cm^{-2} s^{-1}). The value of σ is calculated from the extinction coefficient ε using[55]

$$\sigma = 3.82\times10^{-21}\mathrm{cm}^2 \cdot \varepsilon \quad (B3)$$

using ε in M^{-1} cm^{-1}. For Dendra2, the extinction coefficient is 35,000 M^{-1} cm^{-1} at the peak excitation wavelength of 553 nm (see ref. 31). The cross-section is then 1.3×10^{-16} cm^2. The intensity is estimated using

$$I = \frac{P}{A} \approx \frac{Q}{\pi w_0^2} \quad (B4)$$

where Q is the number of excitation photons per second incident on the sample, A is the area over which they are spread and w_0 is the beam radius (if circular). Q can be calculated from P, the power at the sample in W and wavelength in nm, using

$$Q = P \cdot \lambda_{nm} \cdot 5.04\times10^{15}\mathrm{photons\ s}^{-1} \quad (B5)$$

Plugging into equation (B5) for Dendra2 with 20 mW at 553 nm, $Q=5.6\times10^{16}$ photons s^{-1} and using a beam radius of 10 μm$=10 \times 10^{-4}$ cm, $A=3.1\times10^{-6}$ cm^2, and $I=1.8\times10^{22}$ photons/cm^2s. Using equation (B2), $k_x=2.4\times10^6$/s. Finally, using equation (B1), a detection efficiency of 0.03 (3%) and $\phi_{fl}=0.55$ (see ref. 31), $f_{det} = 4\times10^4$ photons s^{-1} until the molecule photobleaches (which may occur in a fraction of a second). To detect at least 100 photons per frame, we need $N = f_{det}.\tau_{frame} > 100$ or $\tau_{frame} > 100/f_{det}=2.5$ ms. For 1,000 photons per frame, 25-ms frames are needed. Photobleaching ultimately limits the number of detected photons to (on average) $N_{max} \sim \phi_{fl} \cdot \phi_{det}/\phi_B$, where ϕ_B is the photobleaching quantum yield, typically $\sim10^{-5}$ for a fluorophore that is resistant to bleaching. Using $\phi_B=10^{-5}$, we estimate $N_{max} \sim 1{,}650$ for the same quantum yield and detection efficiency used above.

Laser intensities and camera frame rates. Laser intensities (readout and activation) depend on the absorption coefficients and quantum yields for activation and readout for a particular photoactivatable probe. Average intensities at the sample can be estimated approximately (see **Box 1**) by measuring the laser power at the sample using a power meter placed on the sample stage directly above the (dry) objective lens (see Step 12) and dividing by the area illuminated at the sample. The area illuminated can be determined by imaging a solution of conventional fluorophore (see Steps 9 and 10). For fixed samples, the camera frame rate (exposure time) should be adjusted so that, on average, a single molecule is visible for approximately one frame before bleaching, to optimize the number of detected photons per frame and minimize the number of background photons collected. However, for live cell imaging, it is desirable to have molecules visible for multiple frames before bleaching to quantify mobility. In both cases, it is important to read out molecules as quickly as possible while maximizing the number of photons emitted per molecule. Faster acquisitions minimize systematic errors associated with stage drift and cellular movements in live cells. Live cell imaging also requires the acquisition rate to be high enough so that the images of single molecules are not significantly blurred due to the motion of the molecules themselves during each frame. As a rule of thumb, maintain a density of visible molecules per frame of ~ 1 μm^{-2} (values in the range from 0.1 to 5.0 μm^{-2} may be acceptable depending on the circumstances; see caveats below), with molecules, on average, visible for one frame, although in practice approaching this density increases the probability that activated molecules will have overlapping point-spread functions. For example, for molecules distributed randomly at 0.1, 1 and 5 μm^{-2}, molecules will have a nearest neighbor closer than 250 nm approximately 1.5%, 14% and 54% of the time, respectively. Thus, a tradeoff exists between imaging speed and density of localized molecules. Improved algorithms can accommodate higher densities of molecules. Note that the appropriate activation intensity is also a function of the density of inactive molecules. In some cases, as the number of inactive molecules decreases over time, an increase in activation intensity by 10- to 100-fold is required. For example, successful imaging of Dendra2 was achieved at frame rates of ~ 30 Hz, with $\sim 10^4$ W cm^{-2} of 556-nm readout and continuous 405-nm activation (approximately 0.6–6 W cm^{-2}, increased manually as the number of molecules visible on the camera display decreased as a function of time), and effective resolution of ~ 20 nm in ~ 5 min in fixed cells[18]. FPALM imaging of PAGFP in living cells is also possible using $\sim 10^3$ W cm^{-2} of 488-nm readout and $\sim 10^2$ W cm^{-2} of 405-nm activation at frame rates of ~ 10 Hz (see ref. 7).

Faster acquisitions are possible using continuous illumination by the activation laser, although this method may induce additional background fluorescence in the images if the photoactivatable probe is weakly fluorescent in the inactive state or if other background is excited by the activation beam. In this case, using a shutter to apply pulses (either manually or with software control) of the activation laser may be more appropriate. The duration of pulses depends on the activation intensity and the density of inactive molecules, but as with continuous activation illumination, it should be adjusted to achieve a density of visible molecules of ~ 1 μm^{-2}. Longer pulse duration and higher intensity of the activation beam are required as the acquisition progresses (i.e., the density of inactive molecules decreases). As molecules usually photobleach very quickly (within <1 s) under high-intensity illumination, activation pulses may need to be applied very frequently. As mentioned above, when implementing activation procedures to maintain an optimal density of visible molecules, a tradeoff exists between the imaging speed and the occurrence of overlapping single-molecule images. Faster acquisitions are possible with larger numbers of localized molecule per frame, but because activation is a stochastic process, as the density of visible molecules per frame increases, so do the chances that the images of the single molecules will overlap and complicate analysis (or force some frames or portions of frames to be discarded).

Identification of single molecules. During post-acquisition image analysis, the thresholds needed to identify single molecules depend on the number of detected photons, background levels and pixel size. **Figure 3** shows images of single molecules of

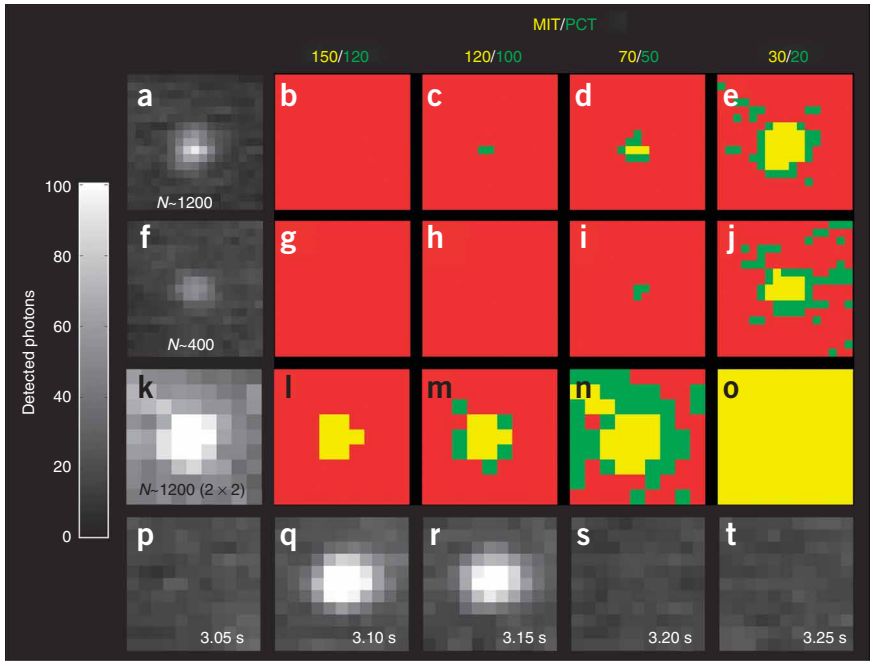

Figure 3 | Identifying single molecules. Images of single molecules of Dendra2-actin from fixed fibroblast cells with different numbers of photons ($\sim$1,200 for **a**–**e**, $\sim$400 for **f**–**j** and $\sim$1,200 for **k**–**o**) and pixel binning (1 × 1 for **a**–**j** and 2 × 2 for **k**–**o**). The color-coded images in **b**–**e**,**g**–**j** and **l**–**o** show the number of pixels above two thresholds (printed at the top of the column) for the molecules shown in **a**,**f** and **k**, respectively. Pixels below both thresholds are red, those above the pixel count threshold (PCT) (green value) but below the minimum intensity threshold (MIT) are shown in green and those above the MIT (yellow value) are shown in yellow. (**p**–**t**) A time series of 50-ms frames cropped around a single dendra2-actin molecule showing stepwise activation (compare **p** with **q**) and stepwise photobleaching (compare **r** with **s**). The pixel color corresponding to the number of detected photons in that pixel is shown by the colorbar (left) for **a**,**f**,**k** and **p**–**t**.

Dendra2-actin from fixed fibroblast cells with different numbers of photons (~1,200 for **Fig. 3a–e** and **k–o**, ~400 for **Fig. 3f–j**) and pixel binning (1 × 1 for **Fig. 3a–j** and 2 × 2 for **Fig. 3k–o**). The key features that suggest an object is a single molecule are the observation of stepwise photobleaching and the size and shape of the image, which should be the same as the diffraction-limited point spread function (PSF). Molecule images should be background-subtracted before identification is attempted. The number of pixels above a certain value will depend on the brightness of that molecule. The color-coded images in **Figure 3** show the number of pixels above two thresholds, printed at the top of each column. Pixels below both thresholds are red, those above the green value are shown in green and those above the yellow value are shown in yellow. Under conditions typical for FPALM and with 80–100 nm effective pixel size at the sample, identification of an object as a single molecule requires that (i) it must have at least one pixel above the minimum intensity threshold (MIT); (ii) it must have at least three pixels above the pixel count threshold (PCT; often 65–85% of the MIT). Suppose the MIT is set to 150 photons, **Figure 3b,g,l** shows that only with 2 × 2 binning do any pixels have >150 photons. The molecules in **Figure 3a,f** would thus both be rejected using this MIT. Although **Figure 3c** shows that two pixels have >100 photons for the molecule shown in **Figure 3a**, none of the pixels in **Figure 3f** have that many (see **Fig. 3h**), and so the molecule in **Figure 3f** would be rejected by that choice of thresholds. **Figure 3d,i** shows that there are at least three pixels above 50 photons, which would allow both molecules in **Figure 3a,f** to pass the PCT, but the molecule in **Figure 3f** would still not pass the MIT. These thresholds would probably not be stringent enough if 2 pixel × 2 pixel binning is being used (**Fig. 3k–o**), as almost all the pixels are above both thresholds in **Figure 3n**. The thresholds of 30 and 20 photons per pixel (**Fig. 3e,j,o**) are too low, as many pixels not part of the molecule are above these values. As a result, it is sometimes difficult to set the thresholds in a way that identifies all molecules correctly. Thus, in many cases, the thresholds must be made stringent enough that a small fraction of molecules is not identified. **Figure 3p–t** shows a time series of 50-ms frames cropped around a single dendra2-actin molecule showing stepwise activation (compare **Fig. 3p** with **3q**) and stepwise photobleaching (compare **Fig. 3r** with **3s**). Discrete transitions between bright and dark states are evidence that an object is a single molecule (emitter).

MATERIALS

REAGENTS

- Photoactivatable probes (see Experimental design)
- Phenol red free growth media (e.g., modified IMEM; GIBCO/Invitrogen, cat. no. 0930119DJ) with serum, if appropriate
- Lipofectamine 2000 (Invitrogen, cat. no. 11668-019)
- Immersion liquid (e.g., HPLC-grade water; Fisher Scientific, cat. no. W5-4)
- Phosphate-buffered saline (PBS; Sigma-Aldrich, cat. no. P3813)
- 4% (wt/vol) paraformaldehyde (PFA) in PBS (USB Corp., cat. no. 19943)

! CAUTION Poison. Wear appropriate protective equipment and avoid contact with skin or eyes.

- Calibration sample (e.g., FluoSpheres, Invitrogen; see REAGENT SETUP)
- Conventional fluorescent dye with appropriate excitation and emission properties to view laser illumination profiles (e.g., Rhodamine B, Sigma-Aldrich, cat. no. R6626 for 556-nm readout and orange/red emission detection)

EQUIPMENT

- Vibration-isolated optics table (model no. 781-451-02R, TMC or similar)
- Inverted fluorescence microscope (IX71, Olympus America)
- High numerical aperture objective lens (see Experimental design)
- ×10 objective lens for alignment (MDPlan 10, Olympus America, or similar)
- Reticle with crosshairs (Electron Microscopy Sciences, cat. no. NE18) for alignment (not essential but helpful)
- Activation laser (see Experimental design)
- Readout laser (see Experimental design)
- Steering mirrors (Thorlabs, cat. no. PF10-03-P01)
- External shutters for each laser (Thorlabs, cat. no. SH05)
- Neutral-density filters to control laser power at the sample (New Focus, cat. no. 5215)
- Dichroic mirror to combine activation laser and readout laser (see Experimental design)
- External lens ($f = +300$ mm) to focus beams at back aperture of objective lens (Thorlabs, cat. no. AC254-300-A1). The use of an achromat lens is useful to ensure that all wavelengths are focused to approximately the same focal plane at the sample but is not strictly required as long as illumination profiles follow the criteria stated below
- Dichroic mirror to separate fluorescence from laser light (see Experimental design)
- Band-pass emission filter(s) to isolate fluorescence from the sample (see Experimental design)
- Long-pass filter to remove activation wavelengths from the microscope lamp (E500LP, Chroma Technology)
- High sensitivity, cooled, EMCCD camera (iXon+ DU897DCS-BV, Andor Technology, or similar. It is also possible to use nonelectron-multiplying camera, but higher readout noise will result in higher background noise)
- Power meter (Thorlabs, cat. no. PM100; or New Focus, cat. no. 3803)
- Sample chambers with coverslip bottom (Labtek II, Nalge-Nunc International Corp.)
- Suitable enclosure for detection path (see EQUIPMENT SETUP)
- Software to control camera (e.g., Solis for cameras made by Andor Technology) or appropriate to camera used
- Software for post-acquisition image analysis such as Matlab (Mathworks), ImageJ (Wayne Rasband) or similar. Software written by the authors in Matlab 7 is available upon request.

REAGENT SETUP

Calibration samples A calibration sample should be used to verify that the setup is able to image single molecules. A simple pair of calibration samples for daily use is (i) a dilute suspension of fluorescent beads dried on a coverslip (or attached to the coverslip through a linker, such as a poly-histidine tag) such that individual beads are separated enough to be individually identified and (ii) a dilute solution of photoactivatable molecules dried on a coverslip. Note that calibration samples should be prepared on clean coverglass to reduce background fluorescence[45]. These samples should be imaged to confirm objects of the expected diffraction-limited size and emission wavelength; the single molecules should also show stepwise photobleaching behavior. Stage drift can be characterized by analyzing the images and localizing the same particle over many frames (see below). After initial setup and check of the system using fluorophore on glass, it is also important to image a sample of known geometry, e.g., sapphire terraces[4], spherical beads[16] or other simple geometry labeled with photoactivatable probes.

Reduction of background fluorescence in immersion water and imaging buffer Localization precision strongly depends on the background noise in the sample (equation 2). Using cooled EMCCD cameras operated at high gain results in a greatly reduced contribution of camera readout noise relative to shot noise from signal and background fluorescence. Background fluorescence from immersion liquids and imaging buffer, such as PBS, can be reduced by exposure to high-intensity UV light. For example, illuminating 25–50 ml of water (or PBS) for 10–20 min with a 500-W UV lamp significantly reduces signal acquired from fluorescent contaminants[46]. Note that UV exposure may create reactive species in PBS and may not be compatible with live cell imaging.

Sample preparation During sample preparation, measures should be taken to reduce sources of cellular autofluorescence that will contribute to background during imaging. Cultured cells should be grown in media free of phenol red (and

other fluorescent compounds) for at least 2–3 d before imaging (or fixation). Note that serum in media also contributes to cellular autofluorescence. Culture dishes containing transfected cells may also need to be wrapped in opaque material during incubation to prevent activation of photoactivatable probes by UV lamps in the incubator or by room lighting. Residual transfection reagents may also contribute to cellular autofluorescence, and so cells should be rinsed thoroughly before fixation or imaging. Fixed samples can be imaged in UV-bleached PBS (see above) to further reduce background fluorescence.

EQUIPMENT SETUP

Construction of FPALM microscope Fluorescence photoactivation localization microscopy relies on precise localization of the positions of single molecules, so the microscope stage, camera, lasers and other optics should be mounted on a vibration-isolated optics table to minimize systematic time-dependent localization errors due to sample stage drift (see below). Mount the activation and readout lasers to the optics table, leaving enough room to include steering mirrors, neutral-density filters, a dichroic mirror and a lens in the excitation path between the lasers and back port of the microscope stand (see **Fig. 2a**). When mounting lens L1 (**Fig. 2a**) in the excitation path, note that the back aperture plane is not always the same as the physical aperture of the objective lens. However, owing to the large Rayleigh range of the focused beam[47], the illumination profile at the sample will be relatively insensitive to small deviations from an exact positioning of L1 at one focal length from the objective lens back aperture plane. However, the lateral position and alignment of the beam with the optical axis (OA) are important. For further information on the behavior of Gaussian beams, see ref. 47. For the ease of combining the activation and readout lasers, it is recommended to include enough steering mirrors in the beam paths, so that each beam has two independent points of adjustment (to allow both the position and angle of each beam to be controlled). Mount the EMCCD camera just outside the side port of the microscope stand. If desired, leave enough room to include additional lenses to increase the overall magnification (see **Fig. 2b**). The detection path must be suitably enclosed (e.g., with lens tube, black cloth and so on) to ensure that stray light does not reach the camera.

Characterization of lateral stage drift Characterize the lateral stability of the microscope stage by imaging immobilized beads at low density (such that single beads are distinguishable) for a period of time longer than the longest expected duration of data acquisition (typically 30 min is sufficient). The number of photons detected per bead per acquisition frame should be as large as possible to minimize localization errors and therefore reflect actual motions of the beads. Localize beads in each frame using standard FPALM analysis (see PROCEDURE) to determine the positions of the beads as a function of time. Generate histograms (for x and y coordinates) of the deviation from the mean position for single beads and determine the standard deviation of the distributions σ_x and σ_y in x and y, respectively, which provide a measure of the lateral drift of the stage over the acquisition time. Alternatively, nonfluorescent beads immobilized in the same way can be imaged using transmitted light, and the image can be inverted and analyzed in a similar way. Axial drift can be quite significant during FPALM acquisition and requires careful immobilization of the sample relative to the stage. Again, immobilized beads can be imaged as a function of time to determine the degree of drift over time, on the basis of how long initially focused objects remain in focus. Manual refocusing is often necessary during long acquisitions unless an automatic focus system is used.

PROCEDURE

Alignment of setup ● TIMING 0.5–2 h

1| Turn on the readout and activation lasers, using neutral-density filters ND1 and ND2 to reduce the power of each to a safe level for alignment (e.g., <1 mW), and then block each beam using shutters SH1 and SH2 (**Fig. 2**). Allow each laser to stabilize.

! CAUTION Always exercise laser safety precautions when aligning lasers.

2| Put the appropriate combination of a dichroic mirror and a band-pass emission filter into the microscope filter cube.

! CAUTION To avoid eye damage, never look through the oculars without confirming that filter combinations are compatible with the lasers in use and will prevent laser light from reaching the eyes. Additionally, it may also be hazardous to look through the oculars when viewing emissions at wavelengths within or beyond the far-red portion of the visible spectrum (where the blink response of the eye to bright light is inadequate). This danger can be avoided by using an appropriately sensitive camera to image the emitted light, rather than looking through the oculars.

3| Using the $\times 10$ objective lens, place the reticle on the sample stage, bring it into focus and align the center of the scale with the center of the field of view (FOV) under Köhler illumination with the lamp (while viewing through the oculars).

4| To align the camera, send the image of the reticle to the camera port of the microscope and adjust the position of the camera (while viewing the camera live video display) to center the image on the display and bring it into focus. This alignment procedure should only need to be completed after initially installing the camera unless the detection pathway changes.

! CAUTION To avoid damaging the camera sensor, perform this procedure with low lamp intensity (well below camera saturation) with the EM gain disabled.

5| Align the readout laser with the center of the FOV by increasing the lamp intensity and refocusing the objective until the image of the reticle is visible on the face of M2 (note that the microscope shutter must now be open). This step should be performed without lens L1 (**Fig. 2**) in the excitation path and the with the activation beam still blocked. The lamp intensity may need to be near maximum for enough light to reach M2 to form a visible image (ensure that the image is not being sent to the camera). Significant refocusing of the objective will also be necessary. Placing a piece of paper on the surface of M2 will increase the visibility of the image of the reticle. Center the readout beam onto the image of the crosshairs using mirror M1 and then block the readout laser. Now project the image of the reticle onto mirror M4, unblock the readout beam and use mirror M2 to align the beam to the crosshairs (at M4). Block the readout beam.

6| To align the activation laser with the readout beam, project the image of the reticle onto dichroic mirror DM1 (**Fig. 2**), unblock the activation laser and use mirror M3 (**Fig. 2**) to center the beam onto the crosshairs (at DM1). Block the activation beam. Now project the image of the reticle onto mirror M4, unblock the activation beam and use dichroic mirror DM1 to center

the activation beam onto the image of the crosshairs (at M4). The activation and readout lasers should now be approximately collinear. Block the activation laser, remove the reticle from the sample stage and turn off the microscope lamp.
▲ CRITICAL STEP When aligning the activation laser, adjustment of optics other than mirror M3 or dichroic mirror DM1 will change the alignment of the readout laser and will require repeating Steps 5 and 6.
? TROUBLESHOOTING

7| To align the lasers to be collinear with each other and the OA, remove the objective lens, unblock the readout laser and adjust mirror M4 so that the readout beam passes through the center of the objective mount, such that it would strike the center of the back aperture of the objective with the objective in place. Rotate the high-NA objective into place to receive the readout laser beam into its back aperture. Set the objective coverslip correction collar, if applicable. Place a concentrated solution (approximately 1–10 μM when observing a diffraction-limited focus, ~100 μM for larger illuminated area after lens L1 is in place) of an appropriate conventional fluorescent dye (see REAGENTS) on the sample stage, illuminated by the readout beam as transmitted by the objective. As the dye is concentrated, the readout beam should be attenuated by several orders of magnitude for this step. If necessary, use mirror M4 to adjust the angle of the readout beam so that the axis of the beam (the center of the cone of illumination) coincides with the OA (**Fig. 2**). The focal spot should be very close to the center of the field and should not move laterally or deform as the objective is translated axially. The readout laser should now be aligned to the center of the FOV and parallel to the OA.
! CAUTION With no objective lens in place, the readout laser remains collimated. To avoid eye damage, do not look directly down into the objective turret.
? TROUBLESHOOTING

8| To align lens L1 to focus the beams at the back aperture, block both beams and mount lens L1 in the beam path at one focal length (i.e., 300 mm) from the back focal plane of the objective lens (see Experimental design). With no objective lens in place, unblock the readout laser and adjust the horizontal and vertical position (perpendicular to the direction of laser propagation) of the lens so that the beam is in focus at the center of the objective mount.
? TROUBLESHOOTING

9| To image the illumination profile of the readout laser, rotate the high-NA objective into place and illuminate the concentrated dye solution with the readout laser. If necessary, make slight adjustments of the position of L1 or the angle of M4 to ensure parallel alignment of the axis of the approximately conical illumination profile with the OA (gross misalignment now requires repeating Steps 5–8). Send the image of the readout-illuminated dye solution (called the readout beam profile) to the camera and obtain a snapshot using the camera software. Block the readout laser.
! CAUTION Image the illumination profile using low laser intensity to avoid damaging the camera sensor and with the EM gain disabled if necessary.
? TROUBLESHOOTING

10| To image the illumination profile of the activation laser, illuminate a concentrated dye solution with the activation laser and view the profile of the activation beam on the camera live video display (with the readout beam now off). If necessary, use dichroic mirror DM1 to adjust the activation laser alignment (while viewing the camera display) to ensure that the illumination profile of the activation laser is concentric with the profile of the illumination profile of the readout beam. A different (usually higher) illumination intensity (adjust with ND2) may be required to produce the same fluorescence intensity using the activation laser, compared with the readout laser. Use the camera software to obtain a snapshot of the activation illumination profile.
? TROUBLESHOOTING

11| To prevent the transmitted lamp light from inadvertently activating the sample, mount a long-pass filter between the microscope lamp and the sample stage. This filter removes activation wavelengths (e.g., <500 nm for Dendra2) from the transmitted light.
■ PAUSE POINT After laser alignment and imaging of illumination profiles, the setup should remain stable for the duration of the experiment. Drift of the alignment can be checked by comparing subsequent illumination profiles with those obtained during alignment.

12| To adjust and measure laser power, with both lasers blocked use neutral-density filters ND1 and ND2 (**Fig. 2**) to adjust the power of each laser to produce an intensity at the sample appropriate for the particular experiment (see Experimental design). With the objective dry, the sample removed and L1 still in place and aligned, measure the transmitted power by placing the power meter on the sample stage directly above (as close as possible to) the objective lens.

13| Use a calibration sample (e.g., photoactivatable molecules dried on a clean cover glass; see REAGENT SETUP) to verify that single molecules can be activated and imaged with the setup. Single molecules can be identified by their size and profile (given

by the diffraction-limited point-spread function) and by their property of stepwise photobleaching (potentially in multiple steps if the molecule is an oligomer).
▲ CRITICAL STEP Focal plane position is crucial when identifying single molecules; molecules that are out of focus by more than ~1 μm will be hard to distinguish from background.
? TROUBLESHOOTING

Data acquisition ● TIMING **1–30 min**

14| Prepare the camera settings for a kinetic series acquisition (using the camera software) by choosing the frame rate such that molecules are bright in each frame at the given laser intensities (see Experimental design). A rule of thumb is that the number of photons in the peak pixel should be at least 5–10 times the background noise in photons[48]. Although the total number of images per acquisition will vary according to the labeling density and imaging speed, initializing an acquisition of ~10,000 frames generally provides an adequate starting point. An acquisition can be manually terminated if the pool of inactive molecules becomes exhausted before acquiring all frames. The format of the resulting image sequence (e.g., a multilayered TIFF) will depend on the camera software used.

15| Place the sample labeled with photoactivatable probes onto the sample stage. View the sample through the oculars using filtered transmitted light (see Step 11) to locate the desired focal plane and ROI. Both lasers should be blocked during this step.
▲ CRITICAL STEP Excess exposure of the sample to laser light should be minimized whenever possible.

16| To confirm the presence of the desired photoactivatable probes in the sample, illuminate the sample with the readout laser while observing through the oculars. Any spontaneous or readout-activated molecules will be visible (usually as small, shimmering or blinking spots) upon illumination with the readout laser only. Single molecules should show stepwise photobleaching, have the expected color of the PAFP being used and be diffraction limited in apparent size. To avoid confusion with background molecules that may also be visible initially, use shutter SH2 (**Fig. 2**) to briefly illuminate (~1 s) the FOV with the activation laser to confirm the presence of photoactivatable molecules. After activation (even after the activation beam has been blocked), an obvious increase in fluorescence should be observed under readout illumination.
? TROUBLESHOOTING

17| To image a particular region, use filtered transmitted light to select a potential ROI and then briefly illuminate the sample with the readout laser, using an activation pulse if necessary (see Step 16). Perform this step efficiently to reduce photobleaching and readout activation of molecules before acquisition has begun. Note that this step may be performed at laser intensities reduced from those required for data acquisition to further reduce loss of molecules. Once an ROI is chosen, close the microscope shutter to avoid any further loss of molecules and, if necessary, return laser intensities to data acquisition levels. Check that shutter SH2 (**Fig. 2**) is in the closed position.
? TROUBLESHOOTING

18| Using the camera software, first begin the kinetic series acquisition and then immediately open the microscope shutter to illuminate the sample with the readout beam. The focus may require adjustment to bring the probe molecules into sharp focus. Initially, spontaneous and readout-activated molecules, as well as background, will be visible. Images acquired before sample illumination or while adjusting the focus should be discarded during analysis. The typical readout laser (shutter) protocol is to have the readout beam illuminate the sample continuously (shutter open). However, alternate protocols may be required for time-lapse imaging (i.e., intermittent periods of frame acquisition during which continuous readout illumination is used, and between which the readout beam is blocked). **Figure 4** illustrates example timing sequences for FPALM acquisitions. For PAFPs with fast readout-induced quenching (such as Dronpa), the activation beam may need to be pulsed, with the readout beam shuttered during each pulse.
? TROUBLESHOOTING

19| Once the average density of visible photoactivatable molecules falls to $< \sim 1\ \mu m^{-2}$, initiate the activation protocol with continuous illumination by the readout laser. Open shutter SH2 to allow continuous illumination by the activation laser (initially at low intensity). Use neutral-density wheel ND2 to increase the activation intensity as the pool of inactive molecules is depleted over time (see Experimental design).
? TROUBLESHOOTING

20| Continue the procedures for readout/activation until a sufficient number (or all) of photoactivatable probes have been imaged. If molecules are still visible after the initial number of frames has been acquired, begin a new kinetic series acquisition. When appropriate, data consisting of multiple acquisitions can be combined into a single sequence for analysis or analyzed separately.
■ PAUSE POINT Image analysis can be performed at any point after data have been acquired.
? TROUBLESHOOTING

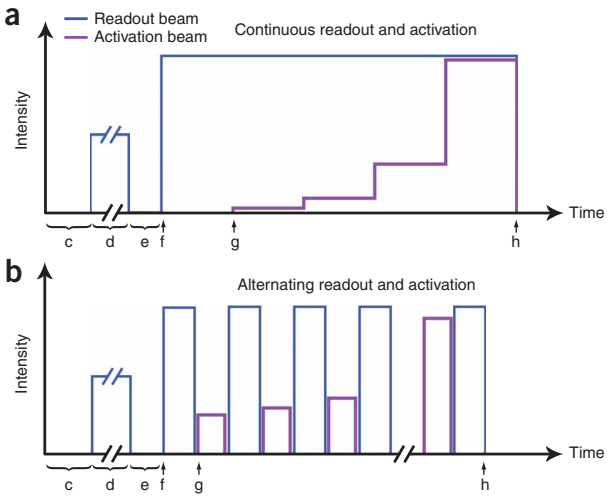

Figure 4 | Example timing sequences for FPALM acquisitions. The readout and activation beam intensities (arbitrary scale) are plotted as a function of time (time axis not to scale), e.g., acquisitions using (**a**) continuous illumination with both beams and (**b**) alternating activation and readout illumination. (**c**) The acquisition settings are prepared. (**d**) The sample is illuminated with the readout beam (at reduced intensity to reduce photobleaching) to select an ROI for imaging. (**e**) The readout beam is shuttered to reduce further photobleaching, and the readout beam intensity is returned to acquisition level before the kinetic series begins. (**f**) The microscope shutter is opened to continuously illuminate the sample with the readout beam and acquisition is begun immediately. (**g**) Activation protocols are initiated once the density of visible molecules decreases to less than $\sim 1\ \mu m^{-2}$. The intensity of the activation beam may be increased over time as the pool of inactive molecules is depleted. (**h**) Both beams are shuttered and data acquisition ends. Approximate duration of steps: **c**, ~1 min; **d**, approximately 1–10 min; **e**, ~30 s; **f**–**h**, approximately from 10 s to 20 min.

Frame-by-frame image analysis and rendering ● TIMING 0.5–4 h

21| After subtracting the zero-light pixel value, convert pixel values to numbers of photons using the camera calibration factor (see Experimental design).

22| Subtract a background profile from the raw image (see **Box 2**). In some rare cases, it may not be necessary to subtract background, but the pixel value offset corresponding to zero light should still be subtracted from each image.

23| To identify and localize single molecules, begin with the brightest pixel in the image and flag all intensity peaks that contain at least one pixel with intensity greater than a suitable threshold (called the MIT) to be considered as a single molecule (see **Fig. 3**). Exclude intensity peaks with significantly overlapping images (closer than ~2 times the width of the point-spread function) from further analysis (or use more advanced localization techniques, e.g., as described in refs. 49,50). Define each identified peak as its own ROI and least-squares fit as a two-dimensional Gaussian to the ROI using the following equation:

$$I(x,y) = I_0 e^{-2[(x-x_0)^2+(y-y_0)^2]/r_0^2} + \text{offset} \quad (1)$$

to determine x_0, y_0, I_0, r_0 and the offset. The intensity-weighted centroid of the ROI can be used as an initial guess for the position (but not as the localized position)[51] to start the fitting routine. Alternatively, to reduce the number of fitting parameters, subtract the minimum pixel intensity from all pixels in the ROI and/or fix r_0 to the measured or calculated value (measured r_0 is preferable to calculated, but r_0 can be estimated using $r_0 \sim \text{FWHM}/1.17 = 0.47\lambda/\text{NA}$ (see ref. 52), where FWHM is the full-width half maximum of the PSF). To determine if the intensity peak is too large or too small to be a single molecule, use additional thresholds. Often, a minimum and maximum number of pixels above a certain intensity level (called the PCT) are used as criteria for identifying single molecules, in addition to the criteria (described above) that at least one pixel must be above a certain value (i.e., the MIT). The PCT is typically less than the intensity of the brightest pixel (see **Fig. 3**). Fitted values of r_0 should also agree with the expected size of the PSF.

? TROUBLESHOOTING

24| Calculate the localization precision (σ_{xy}) for each localized molecule using the following equation[43]:

$$\sigma_{xy}^2 = \frac{s^2 + q^2/12}{N} + \frac{8\pi s^4 b^2}{q^2 N^2} \quad (2)$$

where s is the standard deviation of the PSF ($s = r_0/2$ for a Gaussian). Determine the number of photons detected (N) from each localized molecule by multiplying the Gaussian amplitude in photons (I_0) by the integrated area (in pixels) of a 2D Gaussian with $1/e^2$ radius of r_0 and peak intensity of unity. Determine the background noise per pixel (b) by taking the standard deviation of the intensity (in photons) of an illuminated area in a raw image where no single molecules are visible.
The effective pixel size (q) is calculated as the physical size of a camera pixel (e.g., 16 μm for the Andor iXon + DU897) divided by the total magnification.

? TROUBLESHOOTING

25| Rendering the data can be performed with option A or B.

(A) FPALM rendering

(i) Generate an FPALM image by plotting the positions of localized molecules as two-dimensional Gaussian spots of width proportional to the calculated localization precision and integrated intensity proportional to the number of detected photons.

BOX 2 | BACKGROUND SUBTRACTION

Raw images generally require background subtraction before localizing molecules. A spatially uniform background signal can be subtracted as a zero-level offset (or included as an offset during 2D Gaussian fits; equation 1). However, cell imaging inevitably generates spatially nonuniform background profiles with time-dependent intensities due to photobleaching of cellular autofluorescence. One method to account for a position/time-dependent background signal is to use a weighted summed-widefield profile[7]. To do this, generate a normalized summed-widefield image by summing all raw frames (or the subset of frames analyzed) from an acquisition (after subtraction of the zero-level, the constant pixel value corresponding to zero light). Divide this image by its average pixel value (i.e., normalize to have mean pixel value of 1) to yield a normalized profile containing the position dependence of the background profile. Time dependence of the background profile is implemented by weighting the normalized position-dependent profile by a percentage (typically 90–100%) of the average intensity (after zero-level subtraction) of each individual frame.

Alternatively, the rolling ball algorithm[56] allows the background of each frame to be subtracted independently without relying on any other frames in the acquisition. In this method, a sphere of specified radius is 'rolled' along the underside of the surface generated by the pixel intensities of an image to generate a background subtraction profile. The effect is to filter out objects in the image that are of a size larger than the radius of the sphere. The sphere is chosen to be significantly larger in radius than the diffraction-limited image of a single molecule. This method is implemented in the imaging software ImageJ or can be programmed in a variety of languages.

(B) FPALM density plot

(i) Generate an FPALM density plot by binning all molecules localized within a grid of square pixels of some chosen size (i.e., 25 nm, 50 nm). The intensity of each pixel is then proportional to the number of molecules localized within that pixel. **? TROUBLESHOOTING**

● **TIMING**

Alignment of setup: approximately 0.5–2 h depending on the level of experience

Data acquisition: approximately 1–30 min per acquisition depending on the density of photoactivatable probes and laser intensities used

Frame-by-frame image analysis and data rendering: approximately 0.5–4 h per acquisition depending on the length of acquisition and computer processing abilities. Analysis proceeds more quickly when PAFPs are bright and background levels are low, as finding optimal thresholds is easier in that case.

? TROUBLESHOOTING

Troubleshooting advice can be found in **Table 3**.

TABLE 3 | Troubleshooting table.

Step	Problem	Possible reason	Solution
6 and 10	Readout and activation beams not aligned with each other	Misalignment of steering mirrors	Repeat Steps 5–7 to align the readout and activation beams to a collinear path
7–9	Beams not in the center of the field	Misalignment of steering mirrors	Repeat Steps 5–7 to align the readout and activation beams with the center of the FOV
		Misalignment of focusing lens (L1, see **Fig. 2**)	Repeat Steps 7–9 and align L1 so that the readout laser remains centered to the FOV
		Filter cube, objective or slider slightly out of position	Check whether all movable sliders, the filter cube turret and the objective are 'clicked' in position
		Drift of optics	Check that all optics are firmly clamped down, and that nothing is loose
		Drift of laser direction	Realign beam to center of field, check pointing stability of laser over time
8	Lasers are not focusing at the back aperture of the objective lens	Incorrect positioning of focusing lens (L1, see **Fig. 2**)	Ensure that L1 is at a distance of one focal length from the back aperture plane (not always the same as the physical aperture of the lens)

(continued)

TABLE 3 | Troubleshooting table (continued).

Step	Problem	Possible reason	Solution
9 and 10	Readout or activation laser profile is noncircular	Diode laser $M^2 \gg 1$	Circular beam is not strictly necessary, but if desired, the beam can be made more circular using a spatial filter, or substituting a different laser
		Dirty optics	Clean mirrors and lenses in the excitation path
		Misaligned optics	Repeat Steps 5–10 to align the readout and activation lasers (especially check the position of the beam in the objective back aperture)
9 and 10	Illumination profile is too small/too large	Focal length of focusing lens (L1, see **Fig. 2**) is too large/too small	Use focusing lens of different focal length (e.g., smaller focal lengths give larger illumination areas)
		Initial laser diameter too small/large	Use beam expanders in the excitation path to expand/shrink the beams
10	Readout/activation profiles do not fully overlap	Readout profile is larger/smaller than activation profile	Use beam expanders in the excitation path to expand/shrink one of the beams
13 and 16	Single molecules not visible	Cells in FOV not transfected/labeled	Move to a new region of the sample
		PAFPs have not matured	Wait for 24–48 h after transfection before attempting to image
		Insufficient readout intensity	Increase the intensity of the readout laser
	Ambiguity in identifying single molecules		Confirm stepwise photobleaching, correct size (equal to PSF) (see **Fig. 3**)
	Molecules visible in unlabeled sample or on cover glass	Fluorescent contaminants on coverglass	Prebleach (using readout illumination), or use them as a help to find the coverslip surface, then disregard first few frames of acquisition
		Fluorescent contaminants in buffer	UV-bleach buffer to remove fluorescent contaminants (see REAGENT SETUP)
	Intensity of molecules is lower than expected	Suboptimal filter combination	Ensure that the dichroic mirror and emission filter efficiently transmit fluorescence from the sample
		Low camera gain	Use large electron multiplication factor (approximately 100–300 is typical)
		Low excitation rate of molecules	Increase readout laser intensity (10^3–10^4 W cm^{-2} is typical) or use a wavelength closer to excitation maximum
		Short acquisition time per frame	Increase the acquisition time (not necessarily the same as the time between frames). Estimate time needed to detect at least 100 photons per molecule, assuming a detection efficiency of a few percent (e.g., 5%)
		Objective immersion water evaporated	Reapply immersion water to objective lens

(continued)

TABLE 3 | Troubleshooting table (continued).

Step	Problem	Possible reason	Solution
		Objective NA is too low	Use a higher NA objective
		The image of each molecule is spread over too many camera pixels	Reduce magnification to yield approximately 80–150 nm per pixel effective pixel size in the object focal plane
		Molecules are being quenched	Check sample pH if probe is pH sensitive
13 and 16–18	Too much background signal to distinguish single molecules or achieve desired localization precision	Fluorescent contaminants in immersion liquid or buffer	Use UV-bleached immersion liquid and buffer (see REAGENT SETUP)
		Excessive cellular autofluorescence due to phenol red in growth media	Ensure that cells are grown in phenol red-free media at least 2 d (one cell passage) before imaging
		Excessive cellular autofluorescence due to residual transfection reagents	Wait longer after transfection or increase the number of washes before imaging (or fixation)
		Scattered laser light	Choose dichroic mirror and emission filter for microscope filter cube to more efficiently reflect and reject laser light, respectively
		Bleed through of inactive PAFPs (photoswitchable probes)	Optimize emission filter to collect fluorescence emitted by active molecules or use a different PAFP
		Fluorescence from inactive molecules	Use a different PAFP or lower labeling density (at the cost of reduced densities of localized molecules) or use a different readout wavelength
		Stray light entering detection path	Make sure that the detection path is sufficiently shielded to prevent stray light from reaching the camera, cover sample and reduce room lighting
13, 16 and 19	Density of molecules is too high	Excessive numbers of preactivated molecules	Minimize sample exposure to light, particularly near the activation wavelength
		Excessive readout-induced activation	Lower readout intensity or use a different PAFP (note: PA-GFP has strong readout-induced activation)
		Excessive activation intensity	Lower activation laser intensity
16	Hard to find transfected cells	Low transfection efficiency	Use a photoswitchable probe rather than activatable probe, or use a little bit of activation laser while hunting
	Hard to confirm that cells are transfected	Probe is nonfluorescent before activation	Illuminate briefly with activation laser and confirm increase in fluorescence
16–18	Molecules are out of focus	Wrong focal plane	Adjust focus of objective until images of most single molecules are in sharp focus
		Objective immersion water evaporated	Reapply immersion water to objective lens

(continued)

TABLE 3 | Troubleshooting table (continued).

Step	Problem	Possible reason	Solution
17	Significant photobleaching of molecules occurs before acquisition can be set up	Excessive laser exposure while searching for ROI to image	Use one side of the cell for setup, then move to the other side and start the acquisition
18	Sample drifts or moves with time	Vibration, stage drift	Use drift correction (see EQUIPMENT SETUP)
	z-Focus drifts during acquisition	Vibration, stage drift	Watch the images as they are acquired and focus manually, install an autofocus or reduce acquisition time
		Sample is not exactly horizontal	Apply a small amount of weight on either side of the sample to fix it down
18 and 20	Background increases with time	Contaminated immersion liquid	Use UV-bleached immersion liquid (see REAGENT SETUP)
		Contaminated objective lens	Clean objective thoroughly
23	False negatives in localization routine	Improper thresholding	Reduce thresholds for single-molecule identification (**Fig. 3**)
		Molecules are eliminated by excessive background subtraction	Check that zero-level and percentage of mean are not too large if using summed-widefield method, or that the rolling ball radius is significantly larger than the radius of a single molecule if using rolling ball algorithm (**Box 2**)
	False positives during localization routine (background subtraction)	Improper thresholding	Increase thresholds for single-molecule identification (**Fig. 3**)
		Insufficient background subtraction	Increase zero-level and/or percentage of mean if using summed-widefield method, or decrease the rolling ball radius if using rolling ball algorithm (**Box 2**)
24	Calculated localization precisions seem too small/too big	Incorrect calculation of number of detected photons per molecule or background noise	Check conversion of camera pixel values to photons, check background subtraction levels, background noise levels
		Actual PSF radius is larger than the theoretical PSF (sometimes true for high-NA objectives)	Use the width of the measured PSF (from a fluorescent bead with size much less than the width of the PSF) rather than the calculated PSF. Alternatively, calculations may be checked against the measured localization precision determined by repeatedly measuring the position of an immobilized molecule which is visible for several frames, and taking the standard deviation of that measured position
25	Localized molecules aligned with camera pixels ('pixelization artifact')	Subtracted too much background from raw images	Reanalyze data with reduced background subtraction
		Localized spurious pixels	Increase threshold for single molecule identification (**Fig. 3**)
	Rendered image is too bright (saturated)/too dim	Improper intensity weighting of rendered molecules	Decrease/increase weighting factor and rerender image
	Density of rendered molecules is too sparse	Low fraction of molecules being localized	Lower thresholds for single-molecule identification, subtract less background
		Cells contain too few photoactivatible molecules	Choose cells with higher expression levels, wait longer after transfecting before imaging, use higher activation intensity

ANTICIPATED RESULTS

A typical FPALM image of Dendra2-actin expressed in a fixed mouse fibroblast (T.J.G. and S.T.H., unpublished data) is shown in **Figure 5**. Molecules were localized with a median precision of ~24 nm. In **Figure 5b**, 1,424 molecules were localized over ~2.4 μm^2 (estimating the area of the two fiber bundles) corresponding to a median nearest-neighbor distance (r_{NN}), of ~41 nm, suggesting an effective resolution of

$$\sqrt{\sigma_{xy}^2+r_{NN}^2} = \sqrt{24^2+41^2} \approx 48\text{nm}.$$

The improvement in resolution compared to standard fluorescence microscopy can be seen by comparing the FPALM image (**Fig. 5b**) with the widefield fluorescence image (**Fig. 5c**).

Figure 6 shows another FPALM image of Dendra2-actin expressed in a fixed mouse fibroblast (T.J.G. and S.T.H., unpublished data). In **Figure 6a**, the plotted molecules appear pixelated (appearing in grid-like patterns aligned with the camera pixels) due to failed localizations. The subtraction of too much background and low thresholds can result in too few bright pixels in the images of single molecules, which causes the localization algorithm to fail. In **Figure 6b**, the same data were reanalyzed using the correct background subtraction profile (the zero-level offset subtracted from each image was reduced by 50% of that used for **Fig. 6a**) and pixelization no longer occurs.

Exercise caution in visual interpretation when the density of molecules is low; molecules will often appear clustered or structured in a given way to the eye, but quantitative tests are generally preferable to visual inspection. Note that whenever the number of molecules is small within a given region, the uncertainty in the number of molecules will also be high in that region. Overlays with the widefield fluorescence image or the transmitted light image can be most helpful in determining the context of the structures observed.

Aside from generating super-resolution images, the single molecule information inherent to FPALM and other localization-based imaging methods provides a means for additional analysis. K-test[53] and pair correlation function[54] analysis quantify correlations in the spatial distribution of localized molecules that may be otherwise inaccessible to the eye. Temporal analysis of live cell data also provides diffusion properties at the single-molecule level[7,10].

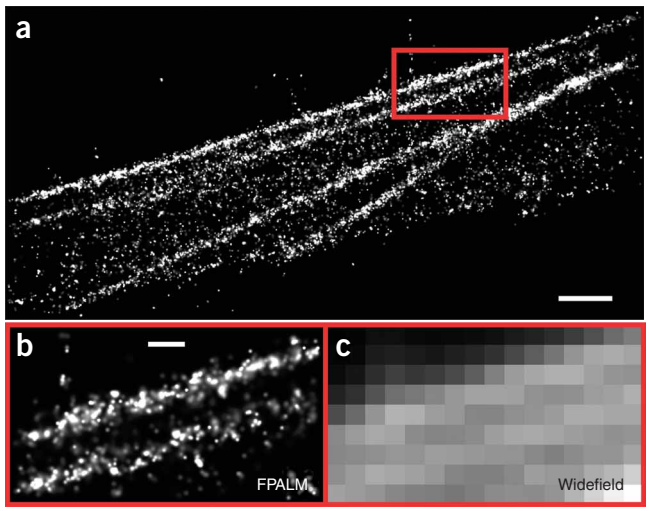

Figure 5 | Typical FPALM image of Dendra2-actin expressed in a fixed mouse fibroblast. (**a**) The distribution of Dendra2-actin molecules (13,256 molecules) localized with ~24-nm median localization precision resolves actin fiber bundles at length scales well below the diffraction limit. Molecules are plotted as 2D Gaussian spots of width proportional to the calculated localization precision and intensity proportional to the number of detected photons. (**b**) Zoom-in of boxed region in (**a**) (1,424 molecules) shows enhancement in resolution over (**c**) conventional widefield fluorescence image. Scale bar, 2 μm for (**a**); 500 nm for (**b**) and (**c**). Brightness and contrast were adjusted linearly in (**c**) for display.

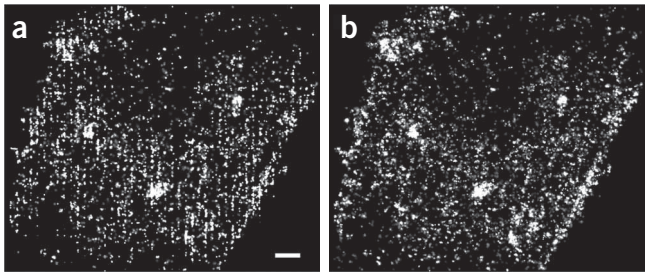

Figure 6 | Illustration of troubleshooting of pixelization artifact in FPALM image of Dendra2-actin expressed in a fixed fibroblast. (**a**) Plots of molecular positions appear pixelated due to failed localizations resulting from too much background subtraction. (**b**) Pixelization no longer occurs after re-analysis using a 50% reduction in the zero level of the background subtraction. Scale bar, 1 μm for (**a**) and (**b**).

ACKNOWLEDGMENTS We thank Christopher Fang-Yen, Paul Blank, Joerg Bewersdorf, Joshua Zimmerberg, George Patterson, Julie Gosse and Michael Mason for useful discussions, Paul Millard and Carol Kim for use of equipment and reagents, Ed Allgeyer, Manasa Gudheti and Siyath Gunewardene for laboratory assistance, Matthew Parent for programming assistance and Thomas Tripp, Tony McGinn and Kyle Jensen for machining services. This work was supported by grants K25-AI-65459 from the National Institute of Allergy and Infectious Diseases (S.T.H.), CHE-0722759 from the National Science Foundation (S.T.H.), start-up funds from the University of Maine (S.T.H.) and by grants GM070358 and GM073913 from the National Institute of General Medical Sciences (V.V.V.).

Published online at http://www.natureprotocols.com
Reprints and permissions information is available online at http://npg.nature.com/reprintsandpermissions

1. Born, M. & Wolf, E. *Principles of Optics: Electromagnetic Theory of Propagation, Interference and Diffraction of Light* (Cambridge University Press, New York, 1997).
2. Hell, S.W. Far-field optical nanoscopy. *Science* **316**, 1153–1158 (2007).
3. Hell, S.W. & Wichmann, J. Breaking the diffraction resolution limit by stimulated emission: stimulated-emission-depletion fluorescence microscopy. *Opt. Lett.* **19**, 780–782 (1994).
4. Hess, S.T., Girirajan, T.P. & Mason, M.D. Ultra-high resolution imaging by fluorescence photoactivation localization microscopy (FPALM). *Biophys. J.* **91**, 4258–4272 (2006).
5. Betzig, E. *et al.* Imaging intracellular fluorescent proteins at nanometer resolution. *Science* **313**, 1642–1645 (2006).
6. Rust, M.J., Bates, M. & Zhuang, X. Sub-diffraction-limit imaging by stochastic optical reconstruction microscopy (STORM). *Nat. Methods* **3**, 793–796 (2006).
7. Hess, S.T. *et al.* Dynamic clustered distribution of hemagglutinin resolved at 40 nm in living cell membranes discriminates between raft theories. *Proc. Natl. Acad. Sci. USA* **104**, 17370–17375 (2007).
8. Geisler, C. *et al.* Resolution of λ/10 in fluorescence microscopy using fast single molecule photo-switching. *Appl. Phys. A* **88**, 223–226 (2007).

9. Flors, C. *et al.* A stroboscopic approach for fast photoactivation-localization microscopy with dronpa mutants. *J. Am. Chem. Soc.* **129**, 13970–13977 (2007).
10. Manley, S. *et al.* High-density mapping of single-molecule trajectories with photoactivated localization microscopy. *Nat. Methods* **5**, 155–157 (2008).
11. Shroff, H., Galbraith, C.G., Galbraith, J.A. & Betzig, E. Live-cell photoactivated localization microscopy of nanoscale adhesion dynamics. *Nat. Methods* **5**, 417–423 (2008).
12. Bates, M., Huang, B., Dempsey, G.T. & Zhuang, X. Multicolor super-resolution imaging with photo-switchable fluorescent probes. *Science* **317**, 1749–1753 (2007).
13. Shroff, H. *et al.* Dual-color superresolution imaging of genetically expressed probes within individual adhesion complexes. *Proc. Natl. Acad. Sci. USA* **104**, 20308–20313 (2007).
14. Bock, H. *et al.* Two-color far-field fluorescence nanoscopy based on photo-switchable emitters. *Appl. Phys. B* **88**, 161–165 (2007).
15. Huang, B., Wang, W., Bates, M. & Zhuang, X. Three-dimensional super-resolution imaging by stochastic optical reconstruction microscopy. *Science* **319**, 810–813 (2008).
16. Juette, M.F. *et al.* Three-dimensional sub-100 nm resolution fluorescence microscopy of thick samples. *Nat. Methods* **5**, 527–529 (2008).
17. Huang, B., Jones, S.A., Brandenburg, B. & Zhuang, X. Whole-cell 3D STORM reveals interactions between cellular structures with nanometer-scale resolution. *Nat. Methods* **5**, 1047–1052 (2008).
18. Gould, T.J. *et al.* Nanoscale imaging of molecular positions and anisotropies. *Nat. Methods* **5**, 1027–1030 (2008).
19. Bates, M., Blosser, T.R. & Zhuang, X. Short-range spectroscopic ruler based on a single-molecule optical switch. *Phys. Rev. Lett.* **94**, 108101 (2005).
20. Lukyanov, K.A., Chudakov, D.M., Lukyanov, S. & Verkhusha, V.V. Innovation: photoactivatable fluorescent proteins. *Nat. Rev. Mol. Cell Biol.* **6**, 885–891 (2005).
21. Patterson, G.H. & Lippincott-Schwartz, J. A photoactivatable GFP for selective photolabeling of proteins and cells. *Science* **297**, 1873–1877 (2002).
22. Chudakov, D.M. *et al.* Photoswitchable cyan fluorescent protein for protein tracking. *Nat. Biotechnol.* **22**, 1435–1439 (2004).
23. Verkhusha, V.V. & Sorkin, A. Conversion of the monomeric red fluorescent protein into a photoactivatable probe. *Chem. Biol.* **12**, 279–85 (2005).
24. Subach, F.V. *et al.* Photoactivatable mCherry for high-resolution two-color fluorescence microscopy. *Nat. Methods* (in press).
25. van Thor, J.J., Gensch, T., Hellingwerf, K.J. & Johnson, L.N. Phototransformation of green fluorescent protein with UV and visible light leads to decarboxylation of glutamate 222. *Nat. Struct. Biol.* **9**, 37–41 (2002).
26. Tsien, R.Y. The green fluorescent protein. *Annu. Rev. Biochem.* **67**, 509–544 (1998).
27. Ando, R., Hama, H., Yamamoto-Hino, M., Mizuno, H. & Miyawaki, A. An optical marker based on the UV-induced green-to-red photoconversion of a fluorescent protein. *Proc. Natl. Acad. Sci. USA* **99**, 12651–12656 (2002).
28. Wiedenmann, J. *et al.* EosFP, a fluorescent marker protein with UV-inducible green-to-red fluorescence conversion. *Proc. Natl. Acad. Sci. USA* **101**, 15905–15910 (2004).
29. Tsutsui, H., Karasawa, S., Shimizu, H., Nukina, N. & Miyawaki, A. Semi-rational engineering of a coral fluorescent protein into an efficient highlighter. *EMBO Rep.* **6**, 233–238 (2005).
30. Gurskaya, N.G. *et al.* Engineering of a monomeric green-to-red photoactivatable fluorescent protein induced by blue light. *Nat. Biotechnol.* **24**, 461–465 (2006).
31. Chudakov, D.M., Lukyanov, S. & Lukyanov, K.A. Tracking intracellular protein movements using photoswitchable fluorescent proteins PS-CFP2 and dendra2. *Nat. Protoc.* **2**, 2024–2032 (2007).
32. Chudakov, D.M. *et al.* Kindling fluorescent proteins for precise in vivo photolabeling. *Nat. Biotechnol.* **21**, 191–194 (2003).
33. Ando, R., Mizuno, H. & Miyawaki, A. Regulated fast nucleocytoplasmic shuttling observed by reversible protein highlighting. *Science* **306**, 1370–1373 (2004).
34. Stiel, A.C. *et al.* 1.8 a bright-state structure of the reversibly switchable fluorescent protein dronpa guides the generation of fast switching variants. *Biochem. J.* **402**, 35–42 (2007).
35. Ando, R., Flors, C., Mizuno, H., Hofkens, J. & Miyawaki, A. Highlighted generation of fluorescence signals using simultaneous two-color irradiation on dronpa mutants. *Biophys. J.* **92**, L97–L99 (2007).
36. Zacharias, D.A., Violin, J.D., Newton, A.C. & Tsien, R.Y. Partitioning of lipid-modified monomeric GFPs into membrane microdomains of live cells. *Science* **296**, 913–916 (2002).
37. Egner, A. *et al.* Fluorescence nanoscopy in whole cells by asynchronous localization of photoswitching emitters. *Biophys. J.* **93**, 3285–3290 (2007).
38. Haupts, U., Maiti, S., Schwille, P. & Webb, W.W. Dynamics of fluorescence fluctuations in green fluorescent protein observed by fluorescence correlation spectroscopy. *Proc. Natl. Acad. Sci. USA* **95**, 13573–13578 (1998).
39. Schwille, P., Kummer, S., Heikal, A.A., Moerner, W.E. & Webb, W.W. Fluorescence correlation spectroscopy reveals fast optical excitation-driven intramolecular dynamics of yellow fluorescent proteins. *Proc. Natl. Acad. Sci. USA* **97**, 151–156 (2000).
40. Heikal, A.A., Hess, S.T., Baird, G.S., Tsien, R.Y. & Webb, W.W. Molecular spectroscopy and dynamics of intrinsically fluorescent proteins: Coral red (dsred) and yellow (citrine). *Proc. Natl. Acad. Sci. USA* **97**, 11996–12001 (2000).
41. Dickson, R.M., Cubitt, A.B., Tsien, R.Y. & Moerner, W.E. On/off blinking and switching behaviour of single molecules of green fluorescent protein. *Nature* **388**, 355–358 (1997).
42. Enderlein, J., Toprak, E. & Selvin, P.R. Polarization effect on position accuracy of fluorophore localization. *Opt. Expr.* **14**, 8111–8120 (2006).
43. Thompson, R.E., Larson, D.R. & Webb, W.W. Precise nanometer localization analysis for individual fluorescent probes. *Biophys. J.* **82**, 2775–2783 (2002).
44. Shaner, N.C., Patterson, G.H. & Davidson, M.W. Advances in fluorescent protein technology. *J. Cell Sci.* **120**, 4247–4260 (2007).
45. Ha, T. Single-molecule fluorescence resonance energy transfer. *Methods* **25**, 78–86 (2001).
46. Hess, S.T., Gould, T.J., Gunewardene, M., Bewersdorf, J. & Mason, M.D. Ultra-high resolution imaging of biomolecules by fluorescence photoactivation localization microscopy (FPALM). In *Methods in Molecular Biology* (eds. Foote, R.S. & Lee, J.W.) in press (Humana Press, Totowa, NJ).
47. Self, S.A. Focusing of spherical Gaussian beams. *Appl. Opt.* **22**, 658 (1983).
48. Currie, L.A. Limits for qualitative detection and quantitative determination. *Anal. Chem.* **40**, 586–593 (1968).
49. Gordon, M.P., Ha, T. & Selvin, P.R. Single-molecule high-resolution imaging with photobleaching. *Proc. Natl. Acad. Sci. USA* **101**, 6462–6465 (2004).
50. Qu, X., Wu, D., Mets, L. & Scherer, N.F. Nanometer-localized multiple single-molecule fluorescence microscopy. *Proc. Natl. Acad. Sci. USA* **101**, 11298–11303 (2004).
51. Cheezum, M.K., Walker, W.F. & Guilford, W.H. Quantitative comparison of algorithms for tracking single fluorescent particles. *Biophys. J.* **81**, 2378–2388 (2001).
52. Pawley, J.B. *Handbook of Biological Confocal Microscopy* (Plenum Press, New York, 1995).
53. Ripley, B.D. Tests of randomness for spatial point patterns. *J. R. Stat. Soc. Ser. B* **41**, 368–374 (1979).
54. Pathria, R.K. *Statistical Mechanics* (Butterworth-Heinemann, Oxford, Boston, 1996).
55. Lakowicz, J.R. *Principles of Fluorescence Spectroscopy* (Springer Science, New York, 2006).
56. Sternberg, S.R. Biomedical image processing. *IEEE Comput.* **16**, 22–34 (1983).